Appl. Phys. B 84, 149–156 (2006)
DOI: 10.1007/s00340-006-2297-8

Applied Physics B
Lasers and Optics

V. KARÁSEK[1]
K. DHOLAKIA[2]
P. ZEMÁNEK[1,✉]

Analysis of optical binding in one dimension

[1] Institute of Scientific Instruments, Academy of Sciences of the Czech Republic, Královopolská 147, 61264 Brno, Czech Republic
[2] School of Physics and Astronomy, University of St. Andrews, North Haugh, Fife, KY16 9SS, Scotland

Received: 1 January 2006/Revised version: 4 May 2006
Published online: 14 June 2006 •

ABSTRACT The redistribution of light between micro- or nanoobjects placed in counter-propagating laser fields leads to their steady-state spatial configurations. Under appropriate conditions, the objects are spatially separated and form optically bound matter. This is a very exciting phenomenon that is still not fully understood. In this article we present a new theoretical model of how to study this phenomenon, which is based on a coupled dipole method particularly amenable to nanoparticle optical binding. Predictions of this model are compared with experimental data and other theoretical models with satisfactory results.

PACS 42.25.-p; 42.50.Vk; 42.68.Mj

1 Introduction

The term 'optical binding' of microparticles refers to a phenomenon where the scattering of light by microobjects combined with the mechanical effects of light that act to confine these objects exhibit and interplay such that a spatial equilibrium distribution of separated mesoscopic objects is obtained. Such equilibrium positions are created by a very weak balance between the optical forces from the incident fields (laser beams) and from the scattered fields generated by the microparticles. Every motional fluctuation of the object modifies the final field distribution and consequently also the equilibrium positions of the objects. Since all the objects are subjects to thermal Brownian motion, it is a great challenge to understand and to describe this phenomenon due to its potential importance for possible self-organisation of a particle array due to this co-operative interaction. Despite the fact that the optical binding was recognised more than ten years ago [1, 2], it was experimentally realised quite recently in a coaxial arrangement [3, 4] with a large inter-particle spacing. However, it is only partially understood from a theoretical standpoint although some models have attempted to describe this phenomenon [4, 5]. The previous theoretical and experimental work was mainly focused on spherical objects having a diameter of several micrometres. In this paper we focus on a different model applicable mainly to sub-micron objects and nanoobjects that is based on the coupled dipole method (CDM) of Purcell and Pennypacker [6], which is also known as the discrete dipole approximation [7]. The main principle of the CDM is to divide a scatterer into smaller parts which can be assumed as individual dipoles. Since these dipoles are much smaller than the light wavelength, Rayleigh scattering is the dominant process. If one takes into account mutual interactions between dipoles and self-interaction of the dipole with itself, a set of linear equations has to be solved to obtain the new spatial distribution of the light [6]. It is assumed that the region occupied by individual dipoles is so small that the field is uniform there. It gives the following condition:

$$|m|kd \leq 1\,, \tag{1}$$

where m is a ratio of refractive indices of the particle and the surrounding medium, k is a wavenumber and d is the shortest distance between neighbouring dipoles. Since this method is computational, its limitations occur if a huge number of dipoles has to be treated. Therefore, it is useful especially for the study of sub-micron objects. Moreover, the CDM is a very flexible method even for objects of arbitrary shape.

2 Theory

We will briefly describe the principle of the CDM, our symbolism of vectorial indexing, generalisation of the CDM for efficient treatment of two or more objects and calculation of optical forces.

2.1 *Theory of* CDM

Several versions of the theory of the CDM are well described [6–10]. The object scattering the incident electromagnetic field is divided into N sufficiently small domains that can be approximated by a point dipole. The dipole placed at the position $\boldsymbol{r}_i$ in the total electric field $\boldsymbol{E}_i$ has polarisability α_i and instantaneous induced complex dipole moment $\boldsymbol{p}_i = \alpha_i \boldsymbol{E}_i$. There exist several modifications of the Clausius–Mosotti expression for the polarisability. A very detailed study of this problem can be found in [11]. The total field $\boldsymbol{E}_i$ is composed of the incident field $\boldsymbol{E}_{\mathrm{inc},i}$ and fields scattered from all other dipoles. The scattered field at $\boldsymbol{r}_i$ from dipole j with

✉ Fax: +420-541-514-402, E-mail: zemanek@isibrno.cz

polarisation $\boldsymbol{p}_j$ is given by $-A_{ij}\boldsymbol{p}_j$, where the radiation matrix A_{ij} has the form [12]

$$A_{ij} = \frac{\exp(\mathrm{i}k\,r_{ij})}{4\pi\varepsilon_0\varepsilon_r r_{ij}} \times \left[k^2\left(\boldsymbol{n}_{ij}\boldsymbol{n}_{ij} - \mathbf{1}_3\right) + \frac{\mathrm{i}k\,r_{ij} - 1}{r_{ij}^2}\left(3\boldsymbol{n}_{ij}\boldsymbol{n}_{ij} - \mathbf{1}_3\right)\right] . \quad (2)$$

Here k is a wavenumber in the medium, $r_{ij} = |\boldsymbol{r}_i - \boldsymbol{r}_j|$, $\boldsymbol{n}_{ij} = (\boldsymbol{r}_i - \boldsymbol{r}_j)/r_{ij}$ and $\mathbf{1}_3$ is the 3×3 identity matrix. Therefore, the total electric field $\boldsymbol{E}_i$ at $\boldsymbol{r}_i$ is expressed as

$$\boldsymbol{E}_i = \boldsymbol{E}_{\mathrm{inc},i} - \sum_{j\neq i} A_{ij}\boldsymbol{p}_j . \quad (3)$$

By setting $A_{ii} \equiv \alpha_i^{-1}\mathbf{1}_3$, the basic equation of the CDM is obtained as a system of $3N$ complex linear equations written in matrix form:

$$A\boldsymbol{p} = \boldsymbol{E}_{\mathrm{inc}} . \quad (4)$$

With increasing number of dipoles the classical methods of solving a system of linear equations (LU Decomposition, Gaussian elimination, etc.) are not applicable. Therefore, we must use one of the several iterative methods (conjugate gradient, bi-conjugate gradient [13]). These methods require calculations of the matrix–vector products $A\boldsymbol{p}^{(k)}$, where $\boldsymbol{p}^{(k)}$ is a kth guess of the polarisations. One such product requires $\mathcal{O}(N^2)$ numerical operations. However this number together with memory storage requirements for a standard number of dipoles (10^3–10^6) easily exceeds present-day computer capacities. Fortunately, this can be overcome by considering the transitional symmetry of dipole locations and using a fast Fourier transform (FFT) [9] algorithm to master such systems.

In this treatment it is assumed that the dipoles are located on a cubic lattice with lattice constant d and size $M \times M \times M$ dipoles. We introduce a bold three-dimensional (3-D) index $\boldsymbol{i}$:

$$\begin{aligned}
&\boldsymbol{i} = (i_x, i_y, i_z) , \quad \text{where} \quad i_x \in \{1, 2, \ldots, M\} ,\\
&i_y \in \{1, 2, \ldots, M\} \quad \text{and} \quad i_z \in \{1, 2, \ldots, M\},\\
&\boldsymbol{r}_i = d\boldsymbol{i} + \boldsymbol{r}_0 ,\\
&\boldsymbol{r}_{ij} = d(\boldsymbol{i} - \boldsymbol{j}), \quad r_{ij} = d|\boldsymbol{i} - \boldsymbol{j}| \quad \text{and}\\
&\boldsymbol{n}_{ij} = (\boldsymbol{i} - \boldsymbol{j})/|\boldsymbol{i} - \boldsymbol{j}| ,
\end{aligned}$$

and therefore the 3×3 matrices A_{ij} depend only on the difference $\boldsymbol{i} - \boldsymbol{j}$. For better clarity, let us explain the mathematical objects in more detail. Vectors $\boldsymbol{p}_j$ for a certain vector index $\boldsymbol{j} = (j_x, j_y, j_z)$ are classical vectors with three components (x, y and z components of the polarisation of the $\boldsymbol{j}$th dipole). Object $\boldsymbol{p}$ is a set of such vectors located in a space at positions given through $\boldsymbol{r}_j$ by a 3-D index $\boldsymbol{j}$. This is analogous to a vector field but the vectors are only evaluated in discrete points labelled by the 3-D index $\boldsymbol{j}$. So, we will call an object $\boldsymbol{p}$ a 3DDVF – a three-dimensional discrete vector field. Similarly, object A_{ij} is a set of tensors evaluated on a six-dimensional (6-D) space given by two 3-D indices $\boldsymbol{i}$ and $\boldsymbol{j}$. The object A_{ij} will be called a 6DDTF – a six-dimensional discrete tensor field. As noted above, dipoles on a cubic lattice A_{ij} depend only on $\boldsymbol{i} - \boldsymbol{j}$ and therefore for the description of radiation tensors there can be used a new object $A'_{\boldsymbol{m}}$, which depends only on one 3-D index $\boldsymbol{m}$. Therefore, $A'_{\boldsymbol{m}}$ is only a 3DDTF:

$$A'_{\boldsymbol{m}} \equiv A_{ij}, \quad \text{for} \quad \boldsymbol{m} = \boldsymbol{i} - \boldsymbol{j} , \quad (5)$$

and consequently the memory requirements for storing this form of radiation tensor are proportional only to $8M^3$ instead of to M^6 for the original A_{ij}. The matrix–vector products $A\boldsymbol{p}^{(k)}$ can now be rewritten in the form of a 3-D convolution:

$$\sum_j{}' A_{ij}\boldsymbol{p}_j^{(k)} = \sum_j{}' A'_{i-j}\boldsymbol{p}_j{}^{(k)}, \quad \text{for all } \boldsymbol{i} . \quad (6)$$

The number of numerical operations is the same for both forms and is proportional to M^6. This problem was solved by Goodman et al. [9]. They used the convolution theorem and the FFT algorithm [13] for evaluation of the convolutions (6), because the FFT algorithm requires only $\mathcal{O}(M^3 \ln M)$ numerical operations.

According to the convolution theorem [13], the Fourier transform of the convolution of two vectors equals the product of the Fourier transforms of those vectors:

$$\boldsymbol{a} \star \boldsymbol{b} = \mathcal{F}^{-1}\left\{\mathcal{F}(\boldsymbol{a}) \cdot \mathcal{F}(\boldsymbol{b})\right\} . \quad (7)$$

The 3-D convolution in (6) consists in fact of six 3-D convolutions of independent components of A. For example, we consider $\boldsymbol{a}$ as a three-dimensional discrete scalar field (3DDSF) made up from $_{xx}$ components of tensors $A'_{\boldsymbol{m}}$ and $\boldsymbol{b}$ as a 3DDSF made up from $_x$ components of $\boldsymbol{p}$:

$$a_{\boldsymbol{m}} = (A'_{xx})_{\boldsymbol{m}} \quad \text{and} \quad b_{\boldsymbol{m}} = (p_x)_{\boldsymbol{m}} . \quad (8)$$

So, instead of the convolutions in (6) we perform Fourier transforms of $\boldsymbol{a}$ and $\boldsymbol{b}$:

$$\hat{a}_{\boldsymbol{n}} \equiv \mathcal{F}(a_{\boldsymbol{m}}) = \sum_{\boldsymbol{m}} a_{\boldsymbol{m}} \exp\left[\frac{\mathrm{i}}{2M}(\boldsymbol{m}\cdot\boldsymbol{n})\right] , \quad (9)$$

$$\hat{b}_{\boldsymbol{n}} \equiv \mathcal{F}(b_{\boldsymbol{m}}) = \sum_{\boldsymbol{m}} b_{\boldsymbol{m}} \exp\left[\frac{\mathrm{i}}{2M}(\boldsymbol{m}\cdot\boldsymbol{n})\right] , \quad (10)$$

and the required result is an inverse Fourier transform of their product:

$$y_{\boldsymbol{m}'} = \sum_{\boldsymbol{n}} \left(\hat{a}_{\boldsymbol{n}} \cdot \hat{b}_{\boldsymbol{n}}\right) \exp\left[\frac{-\mathrm{i}}{2M}\left(\boldsymbol{n}\cdot\boldsymbol{m}'\right)\right] . \quad (11)$$

To the application of the FFT we must add some dimensional considerations. Index $\boldsymbol{m}$ in tensors $A'_{\boldsymbol{m}}$ describes all mutual positions of dipoles located on the lattice and its components fulfil

$$m_x, m_y, m_z \in \{-(M-1), \ldots, 0, 1, \ldots, (M-1)\} .$$

Tensors $A'_{\boldsymbol{m}}$ are symmetric, so they can be described by six independent elements and each such element, e.g. $(A'_{xy})_{\boldsymbol{m}}$, is described by a $2M \times 2M \times 2M$ matrix by zeroing extra elements. Also, we must extend by zeroing extra elements of the components of $\boldsymbol{p}$ to have size $2M \times 2M \times 2M$ because of the

application of the convolution theorem. We set $A'_{(0,0,0)} = 0$. This tensor corresponds to tensors $A_{jj} = \alpha_j^{-1}\mathbf{1}_3$ and this contribution to the field at places $\boldsymbol{r}_i$ by dipoles located at those places is done separately by mere multiplication.

2.2 CDM *applied to several objects*

From the previous sections it is clear that the use of a FFT is crucial to compute efficiently single objects with many dipoles in a cubical lattice. If the object is not a cube but a sphere, the number of dipoles needed to fill the sphere is smaller than in the case of a cube forming the same cubical lattice. For example, a lattice consisting of $30 \times 30 \times 30$ dipoles can be used to model a cube with 27 000 dipoles or a sphere with 14 328 dipoles – both having the same maximal size $30d$, where d is a lattice constant. Therefore, for a sphere the memory must be allocated for $30 \times 30 \times 30$ dipoles even though approximately only one-half of them is used for the field calculations and the rest is in the code labelled as an unoccupied dipole site. This problem would be much worse if two separated objects were considered. A cuboid containing both objects should be considered and all the dipole sites in the space unoccupied by the objects (mainly the space between them) would have to be taken into the computation.

Fortunately, this can be overcome if the total electric field in places corresponding to one object $\mathcal{C}$ is considered as a sum of a field created by dipoles inside this object $\mathcal{C}$ and a field made by dipoles in the distant objects:

$$^{\mathcal{C}}\boldsymbol{E} = {}^{\mathcal{C}}\boldsymbol{E}_{\mathrm{loc}} + {}^{\mathcal{C}}\boldsymbol{E}_{\mathrm{dist}} .$$

Obviously, the first term satisfies the demands of the FFT because it is equivalent to the single object studied in Sect. 2.1. The second term can be analysed using an example with two cubes $\mathcal{C}$ and $\mathcal{D}$ of the same size a, where each of them is formed from $M \times M \times M$ dipoles. Cube $\mathcal{C}$ is separated with respect to $\mathcal{D}$ by a vector $\boldsymbol{Q}$ as seen in Fig. 1. Dipoles belonging to cube $\mathcal{C}$ are indexed by $\boldsymbol{i}$ and dipoles in cube $\mathcal{D}$ by $\boldsymbol{j}$. Therefore, for mutual distances between dipoles belonging to different objects $\boldsymbol{r}_{ij}$, we can write

$$\begin{aligned}
\boldsymbol{r}_{ij} &= \boldsymbol{r}_i - \boldsymbol{r}_j = d(\boldsymbol{i} - \boldsymbol{j}) + \boldsymbol{Q} , \\
r_{ij} &= \sqrt{d^2|\boldsymbol{i} - \boldsymbol{j}|^2 + |\boldsymbol{Q}|^2} , \\
\boldsymbol{n}_{ij} &= \boldsymbol{r}_{ij}/r_{ij} ,
\end{aligned}$$

and they depend only on the difference $\boldsymbol{i} - \boldsymbol{j}$. So, we conclude that the FFT can be used in general for L separated objects modelled by L lattices having $L(L-1)$ mutual interactions described by tensors $^{\vec{\mathcal{D}}\mathcal{C}}A'$, where the letters $\mathcal{C}$ and $\mathcal{D}$ represent two arbitrary objects. Therefore, the unoccupied space between the objects is not considered in the computations and this fact greatly accelerates the calculations and permits consideration of larger objects.

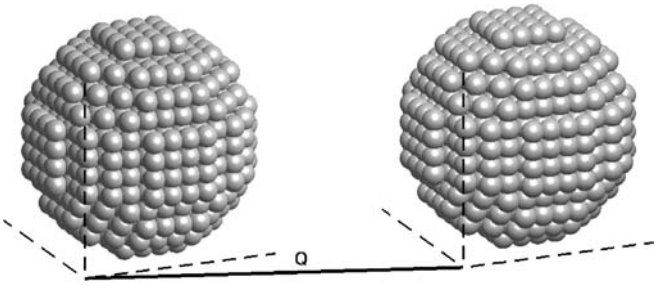

FIGURE 1 An example of two spheres. Each of them is made of $12 \times 12 \times 12$ dipoles in the lattice separated by $\boldsymbol{Q}$

2.3 *Calculation of optical forces using* CDM *for several objects*

There exist two CDM methods suitable for computing forces between dipoles. The first, developed by Draine and Weingartner [7], computes the force from the time-averaged rate of transfer of momentum by the scattered radiation and the second was developed by Hoekstra et al. [10] and uses differentiation of the field. They showed the equivalence of these two methods. We use the second method because it is more suitable for a larger number of dipoles. We modified it slightly for computing with several objects using the same principle as in the case of computing the field. The time-averaged force acting on a dipole $\boldsymbol{i}$ can be written as

$$\langle \boldsymbol{F}_i \rangle = \frac{1}{2}\,\mathrm{Re}\left[(\boldsymbol{p}_i \cdot \nabla)\boldsymbol{E}_i + \mathrm{i}\omega \boldsymbol{p}_i^* \times \boldsymbol{B}_i\right] . \tag{12}$$

The principal step is the splitting of the total force into forces acting from incident and scattered fields [7]. If the incident field can be written in an analytical form (such as a plane wave, Gaussian beam or Bessel beam), we can easily differentiate it and compute the force by (12). Hoekstra et al. [10] showed that forces from the scattered field created by all dipoles $\boldsymbol{p}_j$ located on a cubic lattice can be computed using a FFT, which greatly reduces the memory requirements. Transitional symmetry in expressions for the force between dipoles is preserved if the dipoles are in different objects, too. So, we extended the computation of forces for several objects in the same manner as for the computation of the field.

The total force acting on an object is obtained as the sum of all forces acting on each dipole of the object. These forces come from the incident fields and scattered fields generated by the object itself and by all other objects. For the case of optical binding, we are interested in how this total force acting on a single object depends on the distances among objects, on the objects' optical and geometrical properties, on the parameters of the incident beams and on the properties of the surrounding medium. To find the equilibrium positions, this force must be calculated for various distances among objects with other parameters fixed. The equilibrium position is determined by a zero force and a negative derivative of the force with respect to the axial position.

2.4 CDM *used for two spheres*

It turns out that the optical binding is a very complex problem and therefore we start its examination with the simplest case of two identical dielectric spheres. These spheres are placed in between beam waists of two identical counter-propagating non-interfering Gaussian beams. We assume that both sphere centres are placed on the axis formed by both beams and they are equally distant from the nearest beam waist. We changed the distance between both objects

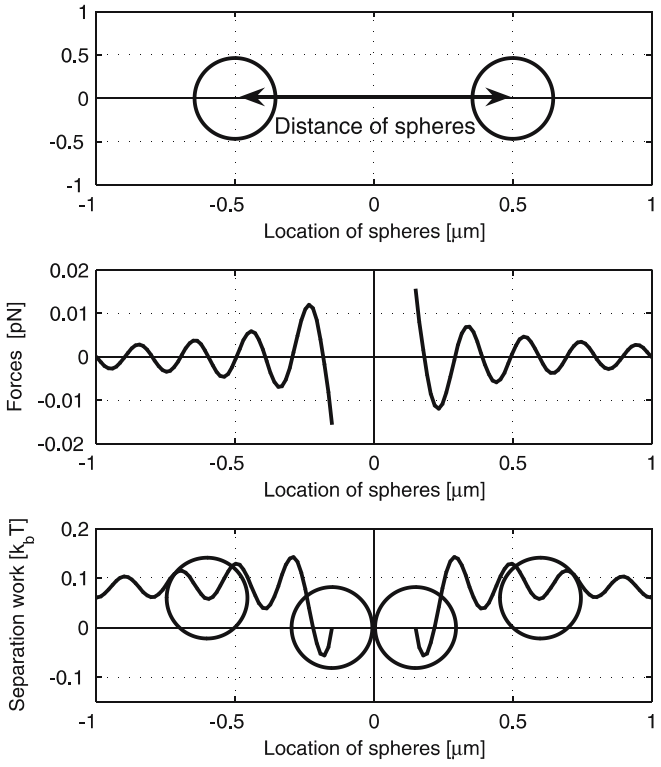

FIGURE 2 Two polystyrene (refractive index equal to 1.59) spheres of diameter 400 nm placed in water are located (as the *top picture* shows) on the common axis of two counter-propagating Gaussian beams having the same beam waist (6 μm), a beam waist separation equal to 100 μm and a power in a single beam of 100 mW. Optical forces acting on each of the spheres were calculated for several inter-sphere distances (the *middle picture*). The *bottom picture* shows the computed work needed to push the spheres apart from each other, done by the forces when separating them from their contact to positions given by their distance apart

and for each of them we calculated the axial component of the force acting on each of the objects. In the chosen symmetrical arrangement the forces acting on the left and right spheres differ only by sign (see Fig. 2). The stable configuration of both spheres occurs for such sphere separations where the force acting on each sphere is equal to zero and the derivative of the force with respect to the axial position is negative. Several stable configurations with different sphere separations can even be found. This is demonstrated in Fig. 2. Since we have not included any other interactions between the spheres except for the interaction between dipoles induced by the incident and scattered fields, the laser power of the beams does not change the equilibrium positions of the spheres. On the other hand, the stable inter-sphere distance is strongly affected by the sphere sizes, the refractive indices of the spheres and the surrounding medium [14] and the parameters of the beams.

3 Measurement of distances between optically bound objects

Experiments were carried out with a counter-propagating single-mode fibre trap. The fibres (Thorlabs HI1060) were illuminated by a diode-pumped ytterbium fiber laser (IPG Photonics, output power 15 W, wavelength $\lambda = 1070$ nm). The beam was linearly polarised, had coherence length less than 1 mm and a collimated beam diameter equal to 5 mm to fill the input aperture of the coupling optics.

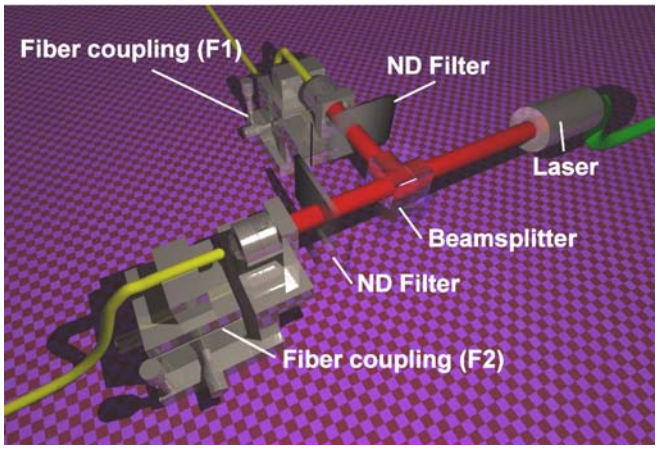

FIGURE 3 Fibre coupling setup: light at 1070 nm from a fiber laser is coupled via ND filters into fibres F1 and F2 to ensure equal power distribution

The laser beam is split with a 50:50 beam-splitter cube into two arms. The optical power in each could be separately adjusted with a variable neutral density filter (ND filter) before entering the fibre coupling optics (see Fig. 3).

By carefully choosing the optical path difference (length difference of the two fibres) well above the coherence length of the laser, standing wave effects were avoided [4]. One fibre (F1) was mounted on a cover slip at a fixed position with respect to the imaging optics; the second fibre (F2) was mounted on an *XYZ* micropositioning stage providing variable distance between the two fibre ends in the range from 70 to 100 μm with an error of ±3 μm.

The imaging system consisted of a ×60 microscope objective (Newport, NA = 0.85) and a CCD camera (Watec WAT 902DM2S) which was connected to a computer with a frame-grabber card to capture the images. The experiment was illuminated from above the cover slip from a distance of 200 mm to ensure coherent illumination and to minimise additional heating of the sample (see Fig. 4).

The observation setup was calibrated by taking images from a microscope calibration grid with a pitch of 100 μm in

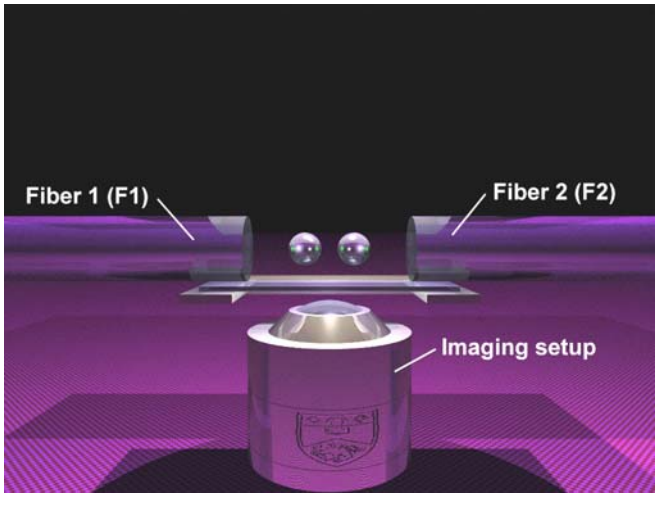

FIGURE 4 Fibre trap side view: the array is formed in the gap between the two fibres F1 and F2

the X and Y plane on top of the cover slip; the error in these measurements was smaller than 1 μm. Data analysis was performed by utilising a LabVIEW script (similar to [15]) with a pattern-recognition algorithm to determine the position of the beads or cells within each frame of a captured movie. The program enables us to average the position of the microspheres up to several hundred measurements dependent on the length of the captured footage.

The investigated arrays were formed by silica microspheres (Bangs Laboratories) of diameter 1.28 μm with an estimated error of ±0.02 μm. Refractive-index measurements on silica microspheres were carried out by Bangs Laboratories using an index-matching technique and the following three results obtained: $n = 1.431$, 1.442 and 1.458 at 588.9 nm. For fused silica the refractive index dependent on the wavelength was approximated to the dispersion equation and showed a shift of $\Delta n = 0.007$ from $n = 1.458$ at 588 nm to $n = 1.451$ at 1070 nm. Furthermore, factors such as the storage time can also alter the refractive index as the bead absorbs water. The refractive index changes from 1.36 to 1.42 (at 575 nm) over a period of 800 h [16]. In our case the refractive index was estimated to be $n = 1.39$.

4 Theoretical conclusions and comparison with experiments

In this paper we focus on a configuration with two optically bound spheres. The distance between them in stable configuration is a parameter that can be measured experimentally and compared with theoretical predictions. Moreover, this parameter should not depend on the intensities of both beams if only the optical forces are concerned. We applied the experimental and theoretical procedures described in the previous sections to obtain the results presented below.

4.1 *Influence of the sphere refractive index and the waist size*

As was described above, it was difficult to determine the refractive index of the silica sphere with sufficient precision. Therefore, we studied theoretically how the distance between spheres in the stable configuration depends on their refractive index. Selected results presented in Fig. 5 show the force acting on the right-hand sphere as the function of the distance between spheres. We considered sphere diameter 1.24 μm, beam waist separation 75 μm and laser power in one beam equal to 100 mW. Three refractive indices n of the sphere were taken for three sizes of beam waists 5.5 μm, 5.7 μm, and 5.9 μm.

The noticeable oscillatory behaviour of the force is caused by the interference of the field coming from a single incident beam but scattered by both spheres. Under proper circumstances these oscillations generate several stable configurations of spheres apart from each other by about half a wavelength. These multiple stable configurations increase the spread of the experimentally detected sphere separations and may complicate the exact comparison with theory.

Figure 5 reveals that the spheres of refractive index 1.38 form a stable configuration only if they are in touch. On the contrary, the spheres of refractive index 1.4 form three well-separated regions of stable positions. But the middle one

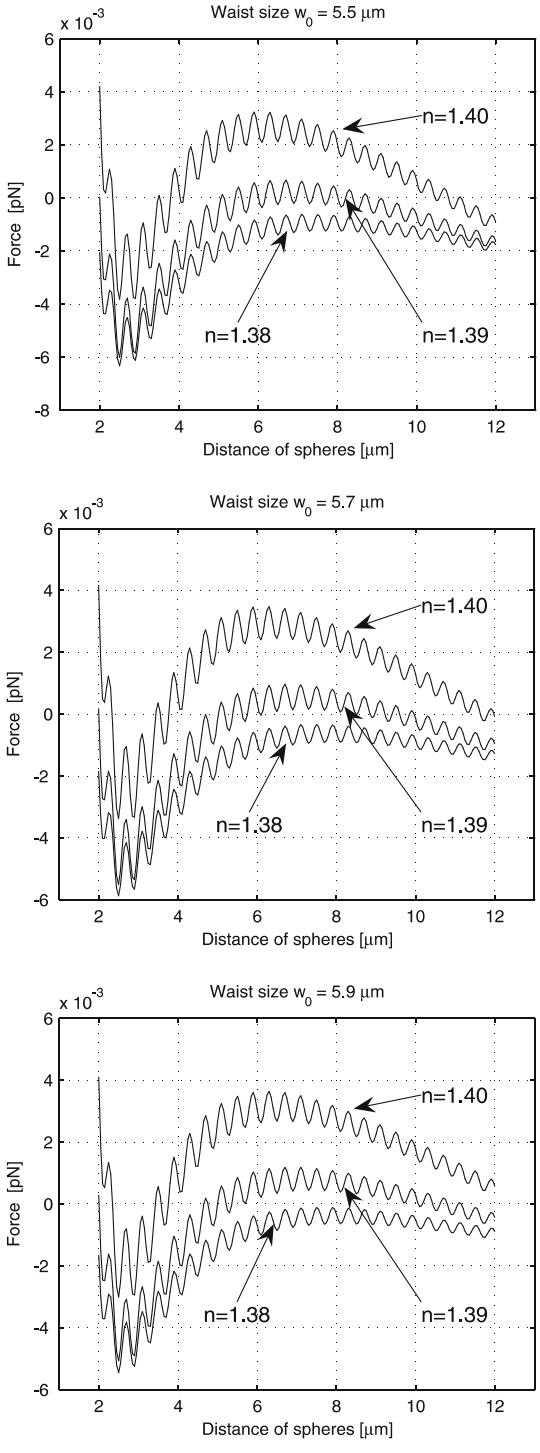

FIGURE 5 The dependence of the total force acting on the right-hand sphere for three different refractive indices n of the spheres. The zero value of the force with a negative slope corresponds to the stable configuration of the spheres. Other parameters used for the calculations were: beam waist of each Gaussian beam 5.5 μm, 5.7 μm and 5.9 μm, distance between beam waists 75 μm, power in one beam 100 mW

would be stable enough only if the kinetic energy of the thermal (Brownian) motion of the spheres was much lower than the work needed to move the spheres to other equilibrium configurations. In the case of the refractive index 1.39 and the beam waist 5.5 μm, only one region of several equilibrium configurations survives but only if the kinetic energy of the

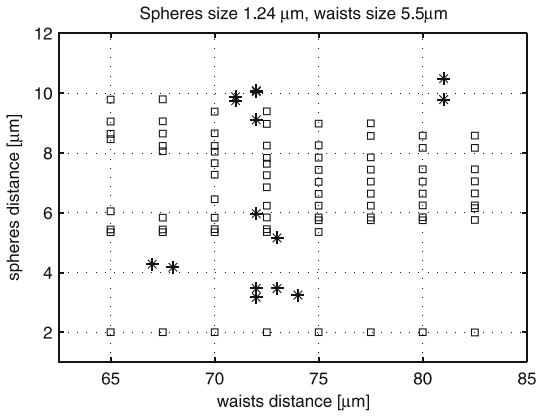

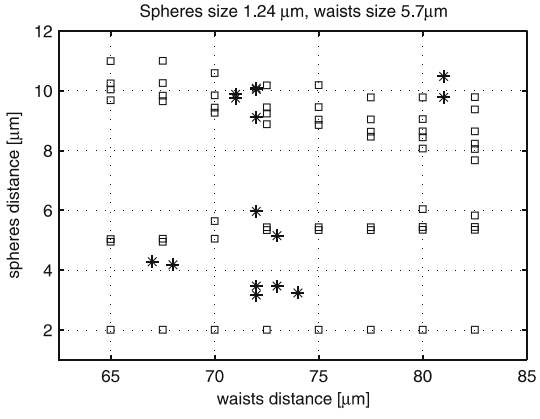

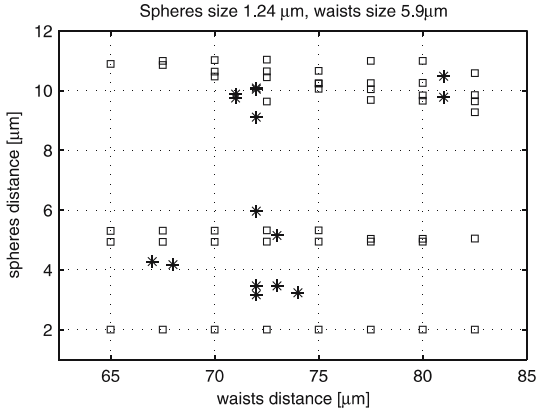

FIGURE 6 The measured distances of spheres (∗) in comparison with CDM simulations (□) for sphere size 1.24 μm and three Gaussian beam waist sizes

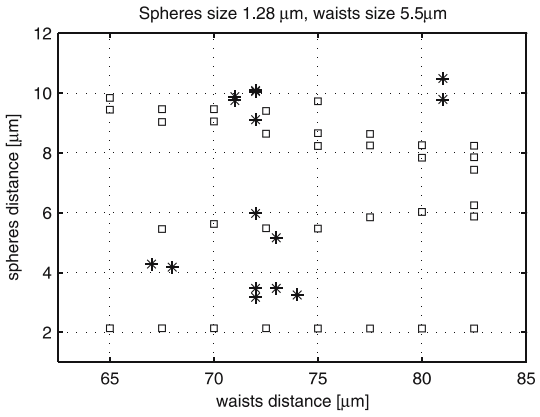

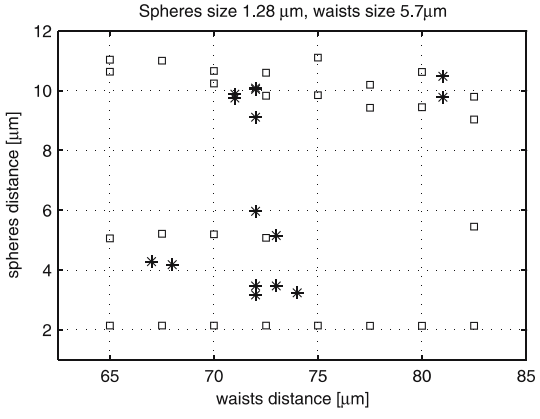

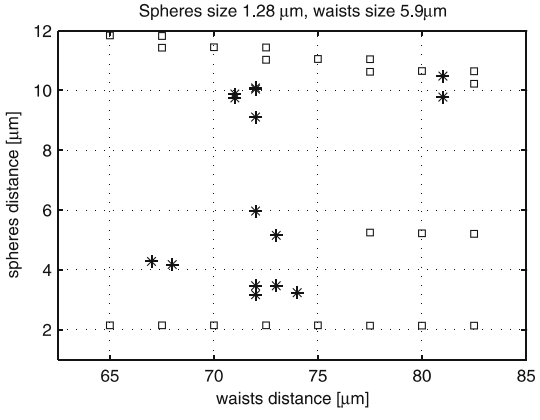

FIGURE 7 The measured distances of spheres (∗) in comparison with CDM simulations (□) for sphere size 1.28 μm and three Gaussian beam waist sizes

thermal (Brownian) motion of the spheres is much lower than the work needed to move the spheres to other equilibrium configurations. Spheres of refractive index 1.39 and other studied beam waists show similar behaviour as those with $n = 1.4$.

These results illustrate how dramatically even 1% changes of the refractive index of the spheres influences the interaction between two optically bound spheres.

4.2 *Comparison with experiment*

Figures 6 and 7 compare the experimental data (∗) with the theoretical predictions of the CDM model (□). Each sub-plot shows one combination of sphere sizes (1.24 μm and 1.28 μm) and beam waists (5.5 μm, 5.7 μm and 5.9 μm) compared with the same experimental data. Repeated measurements with other spheres under the same conditions are shown as 'other' (∗). Based on the studies partially presented in Fig. 5, we choose the refractive index $n = 1.39$.

Three kinds of stable configuration can be distinguished. The first arises for a sphere centre separation of about 2 μm and does not depend too much on the varied parameters. The second occurs for sphere separations larger than 7 μm for the displayed case and it exists for all studied beam waist separations except for the combination of the 1.24-μm sphere with

the 5.5-μm beam waist, where it fused with the third type of stable configuration. With increasing beam waists the stable distances between both spheres increase, too. The same is valid for increasing diameter of the spheres and in the case of the beam waist 5.5 μm the number of possible equilibrium positions is considerably reduced. The third type of stable configuration occurred for sphere separations in between the previous two. Under the studied conditions this one exists for the smaller spheres for all studied beam waist separations. On the contrary, for the bigger spheres it exists only for certain combinations of sizes and separations of beam waists and the bigger the separation the further apart the spheres are settled. The spheres survive in this configuration only if the energy of the thermal fluctuations is lower than the work needed to move the spheres to other equilibrium configurations. This could be the reason why the coincidence with experimental data is so problematic in this region.

The closer the distance between the spheres, the stronger the interactions between them in reality and not all of them come from the light scattering. Therefore, bigger discrepancies between theory and data occurred here because the theory considered only optical forces.

The theoretical results revealed that the distance between the optically bound spheres is extremely sensitive to any of the parameters entering the problem. This substantially complicates the quantitative comparison of experimental and theoretical results because the experimental parameters should be known with high precision. This is not always possible and, as is demonstrated here, changes of the parameters in the order of 1% can dramatically modify the spheres' behaviour. We found a very good coincidence of the theory with the experiments for the configuration where the spheres are far apart. Here we can offer an explanation of why the spread of the measured positions is so large. It is caused by the oscillatory behaviour of the interacting force as shown in Fig. 5. Unfortunately, we have not found an excellent coincidence of the theory with the experiments for configurations where the spheres are closer to each other, but the theory can explain why several different stable configurations experimentally occurred.

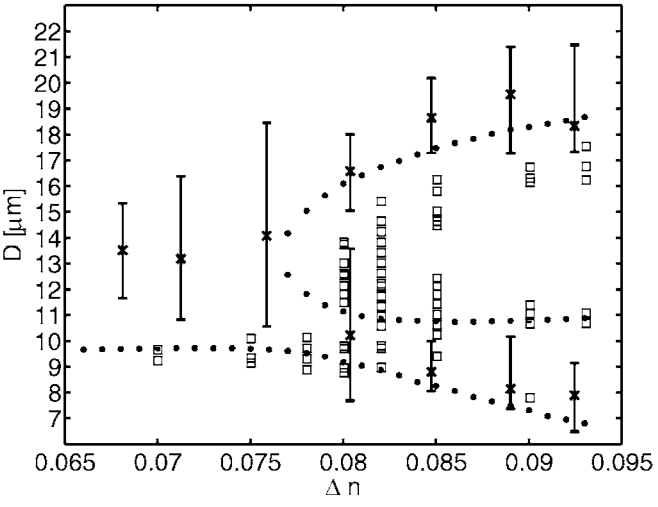

FIGURE 8 Comparison of the distance between two spheres D in the stable configuration predicted by the coupled dipole model with the data presented in [14]. Sphere size is 3 μm, refractive index of the sphere $n = 1.41$, refractive index of the surrounding medium n_m was chosen to fulfil: $\Delta n = n - n_m$, Gaussian beam waist size 3.4 μm, the distance between the beam waists 90 μm. *Dotted curves* show the results of another theoretical model [14], × denotes the measured data with error bars, □ shows the results from the CDM

The sphere size 1.28 μm, beam waist 5.7 μm and sphere refractive index 1.39 give the stable configurations that resemble most of the experimental observations.

The second comparison is based on the data presented by Metzger et al. [14] for a sphere of diameter 3 μm. Figure 8 shows experimental measurements (×) with error bars, their theoretical results (dotted) and our results calculated for the same parameters (□). Contrary to the previous model, the CDM predicts several stable configurations especially in the region where the experimental error bar is the biggest. We believe that it is caused by the fact that the spheres could be stably arranged in several equilibrium positions and this probably led to a bigger spread of the experimental data. The comparison with the theoretical data taken from [14] shows a good coincidence, especially for smaller distances between the spheres.

5 Conclusions

We have presented a new theoretical description using a coupled dipole model approach for the optically bound system of two mesoscopic objects in counter-propagating non-interfering Gaussian beams. This model was applied to the study of how the sphere diameters, beam waist distances and beam waists influence the equilibrium positions of both spheres with respect to each other. The theoretical results were compared with the experimental data. It revealed that the whole phenomenon of optical binding is extremely sensitive to the studied parameters – some of them are very difficult to measure experimentally with sufficient precision. Consequently, we observed a wide variety in the response of the sphere behaviour – from no binding to for example several possible equilibrium positions. Larger quantitative deviations occurred especially for smaller sphere separations, possibly due to effects such as hydrodynamic coupling or appreciable electrostatic interactions between them. Comparison with other theoretical models showed a good coincidence but without the prediction of multiple stable configurations of two spheres.

ACKNOWLEDGEMENTS The authors are obliged to N.K. Metzger for experimental data and for Figs. 3 and 4. This work was partially supported by the EC 6FP NEST ADVENTURE Activity (ATOM3D, Project No. 508 952), ISI IRP (AV0Z20650511), MEYS CR (LC06007) and the European Science Foundation EUROCORES programme (project NOMSAN) with funds from the UK Engineering and Physical Sciences Research Council and from the European Union.

REFERENCES

1 M.M. Burns, J.M. Fournier, J.A. Golovchenko, Phys. Rev. Lett. **63**, 1233 (1989)
2 M.M. Burns, J.M. Fournier, J.A. Golovchenko, Science **249**, 749 (1990)
3 S.A. Tatarkova, A.E. Carruthers, K. Dholakia, Phys. Rev. Lett. **89**, 283 901 (2002)
4 W. Singer, M. Frick, S. Bernet, M. Ritsch-Marte, J. Opt. Soc. Am. B **20**, 1568 (2003)
5 D. McGloin, A.E. Carruthers, K. Dholakia, E.M. Wright, Phys. Rev. E **69**, 021 403 (2004)
6 E.M. Purcell, C.R. Pennypacker, Astrophys. J. **186**, 705 (1973)

7 B. Draine, J.C. Weingartner, Astrophys. J. **470**, 551 (1996)
8 B. Draine, Astrophys. J. **333**, 848 (1988)
9 J.J. Goodman, B.T. Draine, P.J. Flatau, Opt. Lett. **16**, 1198 (1991)
10 A.G. Hoekstra, M. Frijlink, L.B.F.M. Waters, P.M.A. Sloot, J. Opt. Soc. Am. A **18**, 1944 (2001)
11 B. Draine, J. Goodman, Astrophys. J. **405**, 685 (1994)
12 B.T. Draine, P.J. Flatau, J. Opt. Soc. Am. A **11**, 1491 (1994)
13 W.H. Press, S.A. Teukolsky, W.T. Vetterling, B.P. Flannery, Numerical Recipes in C (Cambridge University Press, Cambridge, 1992)
14 N.K. Metzger, K. Dholakia, E.M. Wright, Phys. Rev. Lett. **96**, 068 102 (2006)
15 http://www.st-andrews.ac.uk/~gfm2/tracker.htm
16 M. Ibisate, F. Meseguer, F. Garcia-Santamaria, H. Miguez, C. Lopez, Langmuir **18**, 1942 (2002)